Human Molecular Genetics, 2013, Vol. 22, No. 8 **1525–1538**
doi:10.1093/hmg/ddt003
Advance Access published on January 9, 2013

Enzyme replacement therapy rescues weakness and improves muscle pathology in mice with X-linked myotubular myopathy

Michael W. Lawlor[1,2], Dustin Armstrong[3], Marissa G. Viola[1], Jeffrey J. Widrick[1,4], Hui Meng[2], Robert W. Grange[5], Martin K. Childers[6], Cynthia P. Hsu[1], Michael O'Callaghan[3], Christopher R. Pierson[7], Anna Buj-Bello[8] and Alan H. Beggs[1,*]

[1]Division of Genetics and Program in Genomics, The Manton Center for Orphan Disease Research, Boston Children's Hospital, Harvard Medical School, Boston, MA, USA, [2]Division of Pediatric Pathology, Department of Pathology and Laboratory Medicine, Medical College of Wisconsin, Milwaukee, WI, USA, [3]4s3 Bioscience, Inc., Concord, MA, USA, [4]Department of Physical Medicine and Rehabilitation, Harvard Medical School, and Spaulding Rehabilitation Hospital, Boston, MA, USA, [5]Department of Human Nutrition, Foods and Exercise, College of Agriculture and Life Sciences, Virginia Tech, Blacksburg, VA, USA, [6]Department of Rehabilitation Medicine, University of Washington, Seattle, WA, USA, [7]Department of Laboratory Medicine, Nationwide Children's Hospital, Columbus, OH, USA and [8]Généthon, INSERM, Evry, France

Received October 4, 2012; Revised December 4, 2012; Accepted January 2, 2013

No effective treatment exists for patients with X-linked myotubular myopathy (XLMTM), a fatal congenital muscle disease caused by deficiency of the lipid phosphatase, myotubularin. The *Mtm1*δ4 and *Mtm1* p.R69C mice model severely and moderately symptomatic XLMTM, respectively, due to differences in the degree of myotubularin deficiency. Contractile function of intact extensor digitorum longus (EDL) and soleus muscles from *Mtm1*δ4 mice, which produce no myotubularin, is markedly impaired. Contractile forces generated by chemically skinned single fiber preparations from *Mtm1*δ4 muscle were largely preserved, indicating that weakness was largely due to impaired excitation contraction coupling. *Mtm1* p.R69C mice, which produce small amounts of myotubularin, showed impaired contractile function only in EDL muscles. Short-term replacement of myotubularin with a prototypical targeted protein replacement agent (3E10Fv-MTM1) in *Mtm1*δ4 mice improved contractile function and muscle pathology. These promising findings suggest that even low levels of myotubularin protein replacement can improve the muscle weakness and reverse the pathology that characterizes XLMTM.

INTRODUCTION

X-linked myotubular myopathy (XLMTM) is a severe form of congenital myopathy, with an estimated incidence of 1:50 000 male births (1). Patients with XLMTM often present with severe perinatal weakness that can progress to respiratory failure, but with optimal medical support, some severely affected patients can survive for years (1–3). XLMTM is caused by mutations in the *MTM1* gene that encodes a phosphoinositide phosphatase called myotubularin. Myotubularin has been shown to play a role in multiple cellular processes, including endosomal trafficking (4), excitation contraction coupling (ECC) (5–7), intermediate filament organization (8) and apoptosis (9,10). Muscle biopsy specimens from patients with XLMTM exhibit excessively small muscle fibers with increased numbers of central nuclei and aggregation of organelles within the central regions of many cells (11,12), as well as disorganization of the sarcotubular system on electron microscopy (6).

Two murine models of myotubularin deficiency, *Mtm1*δ4 [also referred to as *Mtm1* knock out (KO) in prior studies

*To whom correspondence should be addressed at: Boston Children's Hospital, 300 Longwood Ave., Boston, MA 02115, USA. Tel: +1 (617) 9192170; Fax: +1 (617) 730-0253; Email: beggs@enders.tch.harvard.edu

(7,13,14)] and *Mtm1* p.R69C mice, provide models of severely and moderately symptomatic myotubularin deficiency, respectively. As the *Mtm1*δ4 mouse is unable to produce any functional myotubularin and the *Mtm1* p.R69C mouse produces small amounts of myotubularin, the dramatic difference in symptomatic severity between these two mice is thought to be due to the presence of small amounts of myotubularin. The range of myotubularin-deficient phenotypes prompted us to investigate pathological findings and corresponding symptomatic severity in different animal models of XLMTM (A) to identify useful prognostic indicators for human muscle biopsies, and (B) to determine whether exogenously administered myotubularin could provide meaningful functional rescue.

Currently, there are no effective therapies to treat muscle weakness in XLMTM patients. Restoration of myotubularin expression using local adeno-associated virus (AAV) gene therapy in myotubularin-deficient mice produces substantial pathological and functional improvement (13), which suggests that treatment of myotubularin-deficient animals with exogenous myotubularin would also be effective. An alternative myotubularin replacement strategy is to use an intracellular delivery technology consisting of a single chain fragment derived from a mouse monoclonal antibody 3E10 (3E10Fv) (15) that is currently in development at 4s3 Bioscience. 3E10Fv fusion proteins penetrate cells through interactions with the equilibrative nucleoside transporter 2 (ENT2) (16) that is expressed at high levels in skeletal muscle (17,18), and these proteins have demonstrated both *in vitro* and *in vivo* functionality (16,19,20). Substantial and preferential skeletal muscle uptake of 3E10Fv has been observed following systemic administration in mice, suggesting that this may be a clinically effective approach to treating myopathies caused by protein deficiencies (21). Therefore, 3E10Fv-fusions with full-length myotubularin protein are predicted to functionally deliver the enzyme to intracellular compartments within skeletal muscle fibers. To test this recombinant therapeutic approach, a 3E10Fv-MTM1 fusion protein (also known as 4s3-001) was generated as a preclinical enzyme replacement product candidate for XLMTM. We initiated a pilot study using intramuscular injections of 3E10Fv-MTM1 to determine the impact of exogenous myotubularin supplementation on the functional and pathological abnormalities seen in *Mtm1*δ4 mice, and provide proof-of-concept evidence for this therapeutic strategy.

RESULTS

*Mtm1*δ4 and *Mtm1* p.R69C mice show distinctive abnormalities of contractile function

Recent work has implicated myofiber size (22) and defects of ECC (6,7) as major contributors to the weakness seen in myotubularin deficiency. While our prior work has established the behavioral and pathological phenotypes of *Mtm1*δ4 (5,13,14) and *Mtm1* p.R69C (23) mice, detailed characterization of contractile function and correlations to specific pathological findings were not performed in those studies. Contractile function of EDL and soleus muscles isolated from male *Mtm1*δ4, *Mtm1* p.R69C and wild-type (WT) littermates were tested to determine the extent and distribution of weakness across these genotypes. Isolated muscle and chemically skinned single fiber segments were tested to determine whether the presence (isolated muscle) and absence (skinned single fiber segments treated with detergent to permeabilize membranes) of ECC changed contractility. When analyzed together, data collected using these techniques can estimate the degree to which abnormalities of fiber size and ECC contribute to muscle weakness in myotubularin deficiency.

Compared with age-matched WT littermates, 6-week-old *Mtm1*δ4 mice displayed marked decreases in maximal contractile-specific force [i.e. force in mN/mm^2 cross-sectional area (CSA)] in isolated soleus and EDL muscles (26 ± 4 and $7 \pm 1\%$ of WT values at 150 Hz, respectively, Fig. 1) ($P < 0.05$). Chemically skinned single fiber studies performed using *Mtm1*δ4 muscle fibers revealed a marked diminution in absolute calcium (Ca^{2+}) activated force of both oxidative (type 1 and 2A) and glycolytic (type 2B) fibers in comparison with age-matched WT fibers (Table 1 and Fig. 2), but these differences in function were less apparent when force was normalized to fiber CSA. Thus, the sarcomeric contractile apparatus in myotubularin-deficient muscle is intact and largely functional, and weakness can be largely attributed to a combination of myofiber smallness and a factor that is removed by the chemical skinning process. As chemical skinning removes the component of contraction produced by ECC and the sarcolemmal membrane, either or both of these factors is responsible for a major component of the weakness observed in myotubularin deficiency.

Contractile deficits in *Mtm1* p.R69C animals were only evident in the intact EDL muscles ($44 \pm 7\%$ of age-matched WT values at 150 Hz, Fig. 1) ($P < 0.05$). *Mtm1* p.R69C soleus muscles did not show a measurable contractile deficit, and generally produced higher contractile-specific force ($139 \pm 14\%$) than was seen in WT animals ($P = \text{NS}$). Contractile function of chemically skinned single fibers from *Mtm1* p.R69C mice was equivalent to age-matched WT fibers irrespective of fiber type, suggesting that the weakness seen in the *Mtm1* p.R69C EDL muscles can also be explained by a combination of fiber size and a factor that is removed by the chemical skinning process (ECC and/or the sarcolemma) (Table 1 and Fig. 2).

Degree of pathology in myotubularin-deficient muscle correlates with function

In comparison with age-matched WT littermates, the EDL and soleus muscles of male *Mtm1*δ4 mice display pathology similar to that described in other muscles of this mouse (5,14), including marked myofiber smallness, increased numbers of centrally nucleated fibers (Fig. 3 and Table 2) and increased numbers of fibers with peripheralization/subsarcolemmal aggregation of mitochondria (24) on nicotinamide adenine dinucleotide (NADH) stain (Table 2 and Fig. 7). In *Mtm1* p.R69C mice at 6 months of age, the EDL muscles displayed similar findings (Table 2). In contrast, the soleus muscle of *Mtm1* p.R69C mice exhibited minimal pathology at the light microscopic level, with fiber sizes comparable with those found in WT littermates and an absence of centrally nucleated fibers or fibers with subsarcolemmal mitochondrial aggregates (Table 2). These findings correlate well with the

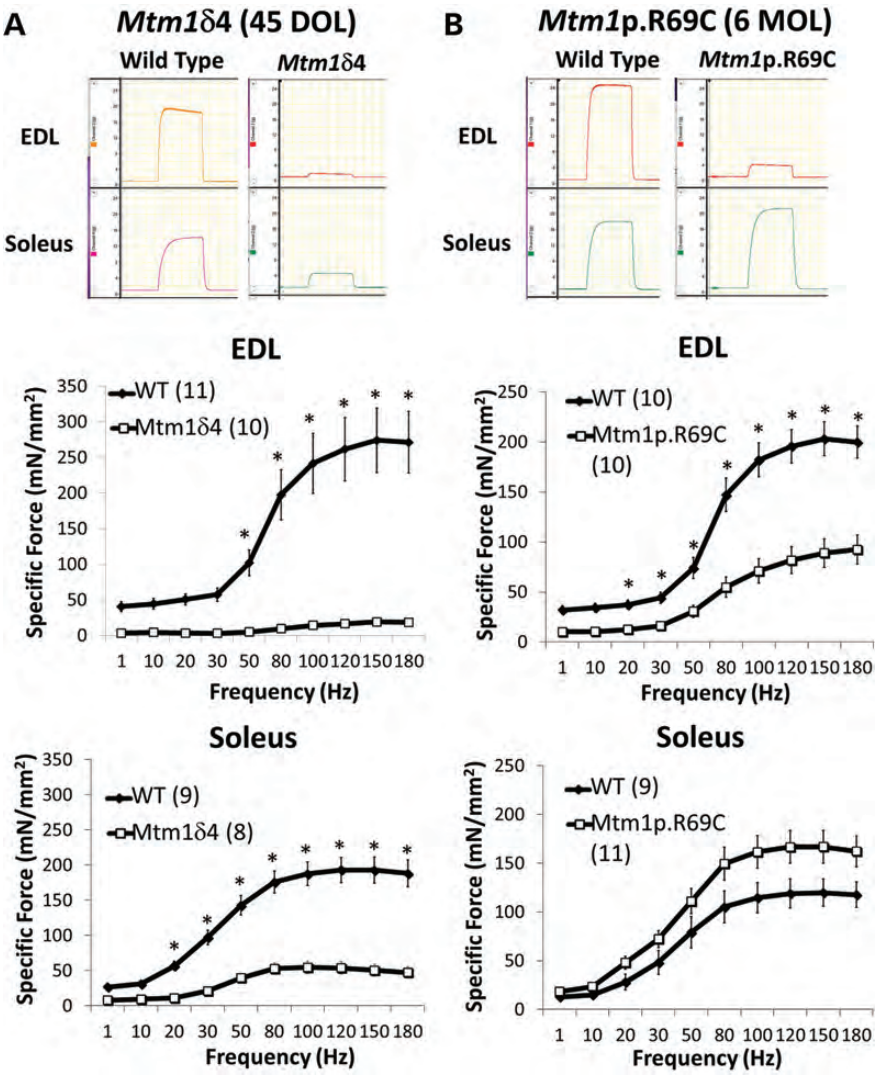

Figure 1. Contractile performance of isolated EDL and soleus muscles in WT and myotubularin deficient mice. *Ex vivo* testing of isolated EDL and soleus muscles evaluates contractile performance over a range of stimulation frequencies, which provides a measurement of contractile force using intact muscle tissue and ECC (51). These studies also provide some insight into fiber-type-specific contractile function, since the soleus muscle is highly enriched for oxidative fibers and the EDL muscle is highly enriched for glycolytic fibers. Contractile performance was assessed by measuring the specific force-frequency relationships in the EDL and soleus muscles of (**A**) 6-week-old WT and *Mtm1*δ4 mice and (**B**) 6-month-old WT and *Mtm1* p.R69C mice. Representative tracings of tetanic responses recorded at a frequency of 150 Hz depict representative maximum (Max) force in each group. Note that the vertical axis of all force tracings have the same scale, but that these measurements do not correct for differences in the cross-sectional area between muscles. Frequency/specific force (or stress) relationships, which account for both contractile force and normalize for the cross-sectional area, are shown for the EDL and soleus muscles of 6-week-old *Mtm1*δ4 and WT mice (left). Frequency/specific force relationships are shown for the EDL and soleus muscles of 6-month-old *Mtm1* p.R69C and WT mice (right). Numbers of replicate muscles studies are in parentheses. $^{*}P < 0.05$.

selective sparing of contractile function in *Mtm1* p.R69C isolated soleus muscles. Immunohistochemical studies confirmed that the EDL muscles of WT, *Mtm1*δ4 and *Mtm1* p.R69C mice were highly enriched in glycolytic (type 2B) fibers, whereas in soleus muscles oxidative (type 1 and 2A) fibers predominated (Table 2 and Fig. 4). Quadriceps muscles from *Mtm1*δ4 and *Mtm1* p.R69C mice are highly predominant in type 2B myofibers, as previously reported (14,23), and the pathology of the quadriceps resembled that seen in the EDL (data not shown).

Distinctive ultrastructural features of myotubularin-deficient myofibers include centrally placed nuclei, aberrant accumulations of glycogen and mitochondria, and a loss of invaginations of the plasma membrane called transverse tubules (T-tubules) that are critical for ECC. These abnormalities have been reported in myotubularin-deficient zebra fish (6), mice (7) and dogs (25). To evaluate the ultrastructural basis for the defective ECC inferred from the mechanical studies, the numbers of triads, T-tubules and longitudinally oriented tubules (L-tubules) were quantified in fibers from isolated muscles evaluated for contractile function (Fig. 3 and Table 2). WT mice at 6 weeks and 6 months of life (MOL) showed similar degrees of sarcotubular organization, with abundant T-tubules and triads and rare L-tubules (Fig. 3 and Table 2). As previously reported (14), 6-week-old *Mtm1*δ4 mice displayed dramatic (45–81%) decreases in the numbers of T-tubules and triads and an increase in L-tubules relative

Table 1. Single fiber cross-sectional area (CSA), Ca^{2+}-activated force, and unloaded shortening velocity (max velocity) data for all groups

Genotype	Fibers quantified	CSA (μm^2)	Force (mN)	Specific force (kN/m^2)	Max velocity (fiber lengths/s)
*Mtm1*δ4 colony, 6 weeks of life					
Slow fibers					
WT	5	1580 ± 130	0.153 ± 0.019	100 ± 15	1.75 ± 0.23
*Mtm1*δ4	4	567 ± 96*	0.035 ± 0.019*	52 ± 23	1.47 ± 0.21
Fast fibers					
WT	39	2844 ± 191	0.190 ± 0.013	68 ± 3	5.45 ± 0.23
*Mtm1*δ4	47	909 ± 63*	0.052 ± 0.004*	57 ± 3*	4.62 ± 0.29*
*Mtm1*p.R69C colony, 6 months of life					
Slow fibers					
WT	10	2303 ± 125	0.276 ± 0.018	120 ± 6	1.47 ± 0.11
*Mtm1*p.R69C	15	2253 ± 126	0.272 ± 0.015	122 ± 5	1.53 ± 0.12
Fast fibers					
WT	23	2400 ± 143	0.248 ± 0.015	104 ± 3	3.34 ± 0.23
*Mtm1*p.R69C	28	2365 ± 162	0.258 ± 0.017	110 ± 3	3.64 ± 0.27

Chemically skinned fibers were activated by direct application of Ca^{2+} (eliminating normal excitation contraction coupling). Specific force normalizes force to unit fiber cross-sectional area. Therefore, comparisons of specific force indicate force capability of equivalent sized fibers in the absence of excitation contraction coupling. Fibers are classified as slow or fast based upon their myosin heavy chain subtypes as determined by gel electrophoresis. Developmental changes in muscle function most likely account for the lower specific forces of fast fibers from the young *Mtm1*δ4 and corresponding WT mice versus the mature *Mtm1*p.R69C mice (54). Data are presented as mean ± SEM.
*$P < 0.05$.

to WT littermates (Fig. 3 and Table 2). Remarkably, muscles from *Mtm1* p.R69C animals also exhibited sarcotubular disorganization similar to that observed in *Mtm1*δ4 mice. The degree of sarcotubular pathology was also similar when comparing the *Mtm1* p.R69C EDL and soleus muscles, despite the dramatic differences in muscle function observed.

Injection of 3E10Fv-MTM1 improves muscle function and pathology in *Mtm1*δ4 mice

A targeted enzyme replacement agent, 3E10Fv-MTM1, has been developed as a means of restoring myotubularin activity to skeletal muscle. Recombinant 3E10Fv-MTM1 retains *in vitro* phosphatase activity similar to reported enzyme function of MTM1-alone (Fig. 5). Thus, to address the question of whether therapeutic delivery of myotubularin would improve muscle function, male *Mtm1*δ4 mice were given intramuscular injections of 3E10Fv-MTM1 (0.1 mg/kg) or equivalent volume of saline into the tibialis anterior (TA) muscle twice weekly between 4 and 6 weeks of life. Intramuscular injection was employed so that both local effects in the injected TA muscle and potentially systemic effects of the disseminated 3E10Fv-MTM1 conjugate could be investigated. The responses in the treated mice indicated that, even at the low dose of 0.1 mg/kg, systemic delivery from the muscle significantly improved muscle function and pathology in treated *Mtm1*δ4 mice. After 2 weeks of treatment, *Mtm1*δ4 mice injected with 3E10Fv-MTM1 displayed improved locomotion over tris buffered saline (TBS)-injected *Mtm1*δ4 littermates, as indicated by increased movement within the cage and a subjective improvement in gait when pairs of animals were evaluated side-by-side (Supplementary Material, Video S1). Functional testing of isolated EDL muscles demonstrated an improvement in strength and established the efficacy of the drug in the injection area. The mean tetanic normalized-specific force of 3E10Fv-MTM1-treated EDLs was 50.0 mN/mm^2 (range = 30.5–92.5 mN/mm^2), or 386% of mean saline-injected muscle values (12.9 mN/mm^2, range 1.7–31.7 mN/mm^2), and 18% of untreated age-matched WT values (274.0 mN/mm^2, range 93.3–554 mN/mm^2) (Fig. 6). The locally injected TA muscles did not show differences in disease pathology at the light microscopic level (Table 3 and Fig. 7), but ultrastructural evaluation of tested EDL muscles revealed an increase in the number of triads and T-tubules, with no significant differences in L-tubules in 3E10Fv-MTM1-injected mice compared with mice treated with TBS alone (Fig. 6 and Table 3). The control condition, unconjugated 3E10Fv-alone, also moderately improved contractile function in isolated EDL muscles of *Mtm1*δ4 mice, although there was no obvious clinical improvement in gait and ambulation such as that seen in 3E10Fv-MTM1-treated animals. EDL muscles from animals injected with 3E10Fv-alone produced mean tetanic normalized-specific force values of 29.6 mN/mm^2, which corresponds to 229% of TBS-injected values and 59% of 3E10Fv-MTM1-injected values (Fig. 6). Statistical evaluation of these data using a two-way ANOVA revealed a significant difference between 3E10Fv-MTM1 and TBS-injected groups ($P < 0.01$), but no statistically significant difference when comparing 3E10Fv-alone to either 3E10Fv-MTM1 or to TBS injection. While injection of 3E10Fv-alone did not affect the pathology of the TA muscles at the light microscopic level, EDL muscles from 3E10Fv-alone-injected animals actually trended toward an increase in sarcotubular disorganization, as indicated by fewer T-tubules and triads and increased L-tubules, in comparison with TBS-injected mice (Fig. 6 and Table 3, P = ns).

DISCUSSION

ECC and defective sarcotubular organization in myotubularin deficiency

The physiological assays performed in this study indicate that factors sensitive to the chemical skinning process, such as ECC or the contribution of the sarcolemmal membrane, are a

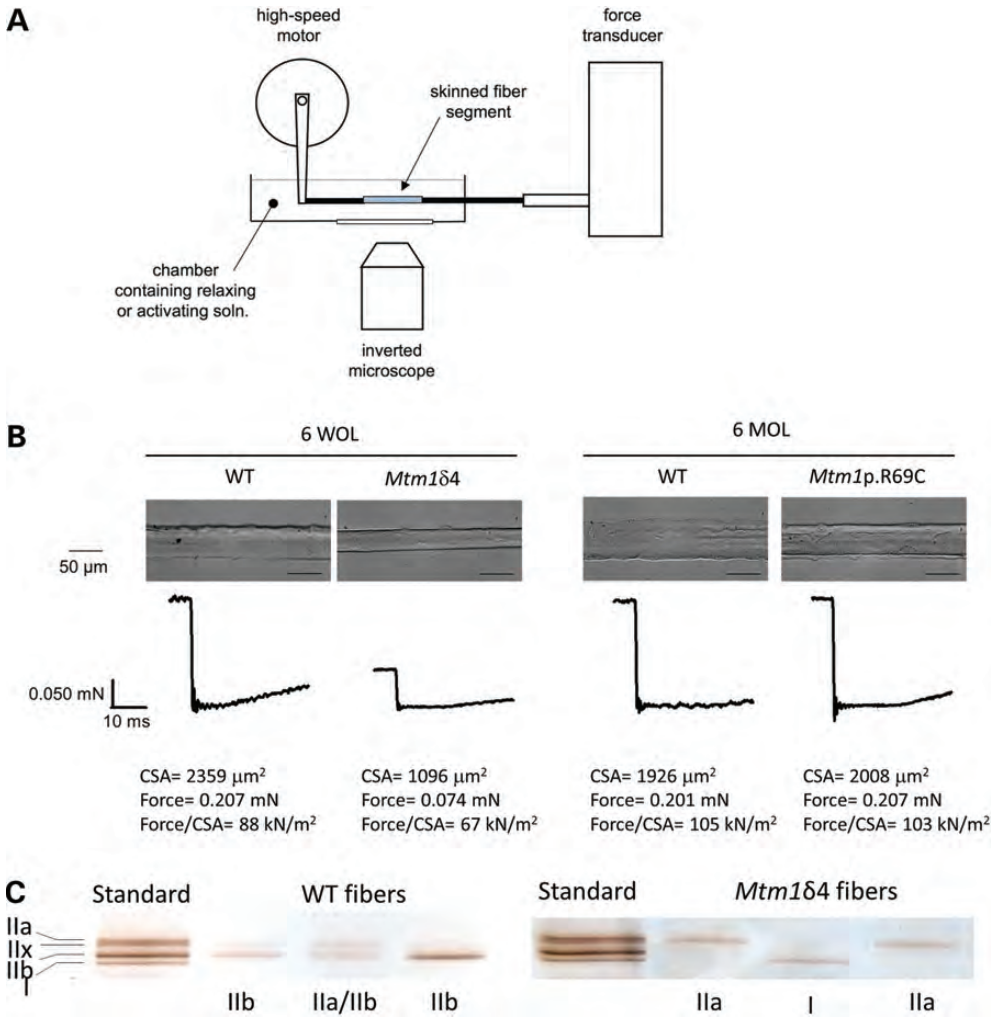

Figure 2. Skinned single fiber studies in WT and myotubularin-deficient mice. Chemically skinned single fiber preparations were performed to evaluate contractile performance independent of excitation contraction coupling. Chemically skinned single fiber preparations evaluate the contractile performance of single myofibers using exogenous calcium, which allows the measurement of contractile function independent of ECC. Force measurements can then be assessed with respect to the fiber cross-sectional area (CSA) to evaluate the impact of fiber size on contractile force. (**A**) Diagram of the equipment used in performing skinned single fiber studies. (**B**) Representative photographs and force measurements from fibers isolated from WT and myotubularin-deficient mice at 6 weeks of life (WOL) and 6 months of life (MOL). Data from these studies are summarized in Table 1. (**C**) Following force measurement, the myosin isoform (type I, IIa, IIb or IIx) expressed by the tested fiber was determined by gel electrophoresis and silver staining, and fiber type was determined by comparison with a standard.

major functional issue in myotubularin deficiency. Using whole muscle testing, *Mtm1*δ4 tetanic contractile force was considerably impaired, but normalization of these values to muscle CSA revealed that only a minor component of this weakness was explainable by differences in muscle size. Relatively preserved contractile function in the chemically skinned single fiber experiments implicated ECC and/or the sarcolemma as the factor responsible for the majority of the observed weakness in myotubularin-deficient animals. Given the reported abnormalities of sarcotubular organization (6,7), Ca^{2+} currents (7), Ca^{2+} channel function(7) and depolarization-induced contraction of single myofibers (6), it is extremely likely that abnormalities of ECC account for most or all of this 'chemical skinning-sensitive' component of weakness. Additionally, EDL muscles showed more dramatic functional impairment than the soleus muscles, suggesting that fast/glycolytic fibers are more sensitive than slow/oxidative fibers to the ECC abnormalities produced by myotubularin deficiency. Our functional studies indicate that ECC abnormalities, which correlated with ultrastructural defects at the triads where myotubularin is localized (13), point to a key feature of myotubularin deficiency and potential therapeutic strategies for XLMTM. Thus, successful treatment modalities must address ECC to maximize their potential benefit. This finding is supported by our prior study using a soluble activin type IIB receptor (ActRIIB-mFc) in *Mtm1*δ4 mice, which produced dramatic improvement in myofiber size, yet less substantial improvements in muscle function (14). The functional and pathological differences observed between *Mtm1* p.R69C EDL and soleus muscles can likely be explained by differences in fiber-type populations between these two muscles, as the EDL muscles were highly enriched for glycolytic fibers and the soleus muscles were highly enriched for oxidative fibers (Fig. 4). Interestingly, while the degree of pathology at the light microscopic level (including

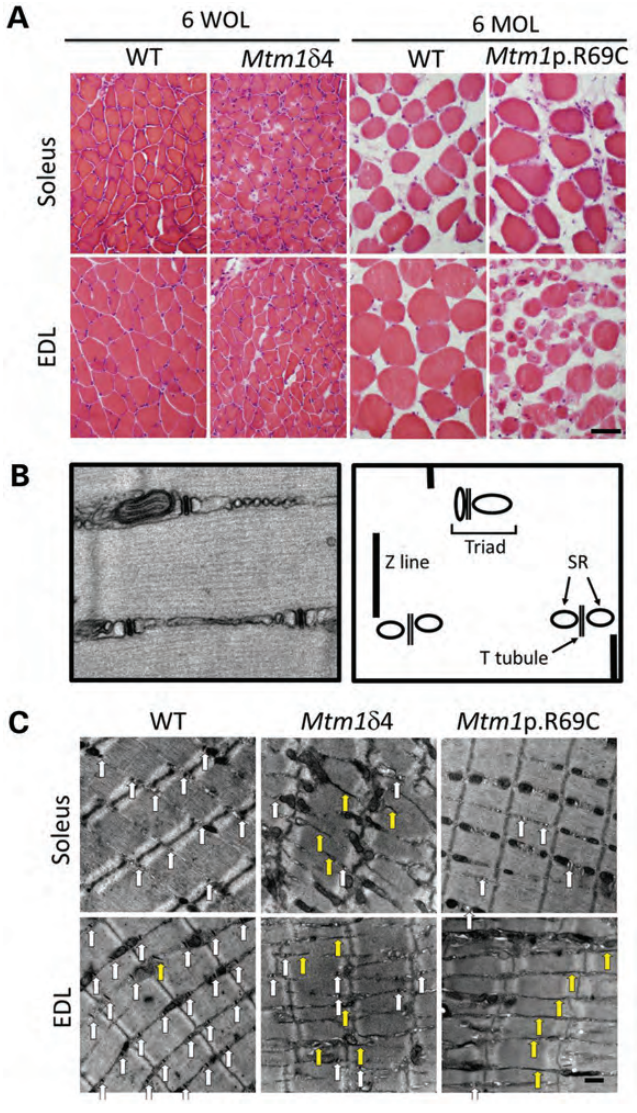

Figure 3. Light microscopic pathology in myotubularin-deficient mice is dependent on mouse strain and the muscle examined. (**A**) Hematoxylin and eosin staining of EDL and soleus muscles from Mtm1δ4, Mtm1 p.R69C or age-matched WT littermate mice display variable levels of myofiber smallness and centrally nucleated fibers. Note that differences in fiber size when comparing the two WT populations is due to the normal growth between 6 weeks of life (WOL) and 6 months of life (MOL). (**B**) To evaluate sarcotubular organization at the ultrastructural level, the number of triads, T-tubules and L-tubules were quantified from longitudinal sections of EDL and soleus muscles from WT and *Mtm1*δ4 animals at six WOL and WT and *Mtm1* p.R69C animals at six MOL. A picture and diagram of the normal sarcotubular architecture from a 6-week-old WT mouse is shown. (**C**) Representative images (×9300 magnification) of longitudinal sections of 6-week-old WT and *Mtm1*δ4 mice, which allow the quantification of T-tubules (white arrows) and L-tubules (yellow arrows). Representative images from a 6-month-old *Mtm1* p.R69C mouse are also shown for comparison. Bar = 50 μm in (A) and 500 nm in (C).

fiber size and the number of fibers with internal nuclei and/or subsarcolemmal mitochondrial aggregates) was different when comparing the *Mtm1* p.R69C EDL and soleus muscles, the degree of sarcotubular disorganization observed at the ultrastructural level was equivalent (Fig. 3 and Table 2). While this finding does not support the use of sarcotubular organization as an indicator of functional capacity, it is possible that the small amount of myotubularin found in *Mtm1* p.R69C mice allows adequate use of the ECC machinery in oxidative fibers. The relative sparing of the soleus muscle in terms of fiber size and contractile function is at odds with the findings of Bevilacqua *et al*., who reported that the soleus muscle was the most severely affected muscle in the lower legs of four patients with late-onset centronuclear myopathy due to *MTM1* mutations (24); however, this may simply reflect species differences between mice and humans. The relationships between myotubularin levels, fiber type, sarcotubular organization and contractile function will be further studied as we continue our treatment studies and improve our methods for documenting myotubularin levels in 3E10Fv-MTM1-treated muscles.

Myotubularin as a candidate for gene- or protein-replacement

The lack of effective therapies to treat muscle weakness in XLMTM patients has left patients and their families only with options for supportive respiratory and orthopedic management. Treatment approaches designed to counteract hypotrophic signaling, such as myostatin-inhibition or ActRIIB-receptor decoy (14), may stimulate transient muscle growth and some symptomatic improvement, but they do not correct the underlying biochemical defects related to myotubularin deficiency. Messenger RNA rescue technologies designed to induce stop codon read-through may be effective for ∼20% of XLMTM patients, but the low incidence of XLMTM and its mutational heterogeneity make this treatment method currently impractical (26). AAV-based gene therapy, which offers the advantage of directly replacing myotubularin, has, however, shown promise when tested in myotubularin KO mice (13). Local administration of AAV1-*Mtm1* in myotubularin KO mice produced a dramatic improvement in pathology and isometric force production in targeted muscles (13), indicating that post-natal replacement of myotubularin is capable of reversing both the structural and functional consequences of myotubularin deficiency. Systemically delivered recombinant myotubularin would provide flexibility in dosing, and this strategy has been successfully employed in other enzyme replacement therapies; including, Myozyme®, Fabrazyme® and Cerezyme® (27). Myotubularin is a cytoplasmic enzyme that is not predicted to have mannosylation, nor does it circulate in the bloodstream (28). Therefore, to target myotubularin to the cytoplasmic compartment of skeletal muscle fibers, it must be chemically conjugated or genetically fused to a moiety capable of specifically targeting and traversing the skeletal muscle sarcolemma. Fortunately, myotubularin retains phosphoinositol (3,4,5)-trisphosphate phosphatase activity following fusion to other proteins including purification tags and fluorescent reporters (29–31). Given these factors and the existence of an easily testable murine XLMTM model, myotubularin is an excellent candidate for proof-of-concept studies for targeted protein replacement using 3E10Fv. Ideally, this delivery strategy will also be useful for a host of other indications that require the specific delivery of proteins to skeletal muscle.

Table 2. Quantification of histological and ultrastructural findings

Genotype/muscle	Fiber size (μm)	% Fibers with internal nuclei	% Fibers with subsarcolemmal mitochondrial aggregates	% Glycolytic fibers (type 2B)
*Mtm1*δ4 colony, 6 weeks of life				
WT soleus	28.90 ± 2.99	0.39 ± 0.23	0.00 ± 0.00	1.64 ± 1.47
*Mtm1*δ4 soleus	28.45 ± 2.46	6.04 ± 1.85*	7.01 ± 3.26*	0.43 ± 0.43
WT EDL	34.02 ± 3.52	0.16 ± 0.10	0.05 ± 0.05	67.97 ± 4.05
*Mtm1*δ4 EDL	24.37 ± 1.78	6.59 ± 3.47*	9.03 ± 0.91*	74.11 ± 7.89
*Mtm1*p.R69C colony, 6 months of life				
WT soleus	48.39 ± 2.54	0.50 ± 0.17	0.12 ± 0.12	2.18 ± 1.01
*Mtm1*p.R69C soleus	40.81 ± 2.39	0.69 ± 0.32	0.11 ± 0.11	0.88 ± 0.60
WT EDL	49.25 ± 3.56	0.47 ± 0.16	0.00 ± 0.00	75.00 ± 2.08
*Mtm1*p.R69C EDL	16.43 ± 3.14*	16.43 ± 3.14*	3.99 ± 0.46*	84.58 ± 3.20
Genotype	Fibers quantified	Triads/field	T-Tubules/field	L-Tubules/field
*Mtm1*δ4 colony, 6 weeks of life				
Soleus muscles				
WT	20	10.25 + 1.44	10.25 + 1.43	0.20 + 0.09
*Mtm1*δ4	15	4.52 + 1.75*	4.26 + 1.72*	2.86 + 0.47*
EDL muscles				
WT	22	19.36 + 1.65	19.09 + 1.63	0.59 + 0.29
*Mtm1*δ4	30	3.83 + 0.87*	3.66 + 0.86*	4.83 + 0.49*
*Mtm1*p.R69C colony, 6 months of life				
Soleus muscles				
WT	10	13.4 + 3.04	14.30 + 2.78	0.40 + 0.22
*Mtm1*p.R69C	22	3.54 + 0.94*	4.00 + 0.92*	1.36 + 0.34*
EDL muscles				
WT	12	29.45 + 1.44	29.27 + 1.48	0.45 + 0.15
*Mtm1*p.R69C	36	3.11 + 0.71*	2.81 + 0.62*	4.78 + 0.95*

Data are presented as the mean ± SEM.
*$P < 0.05$.

The potential of 3E10Fv-MTM1 as a therapeutic agent in myotubularin deficiency

The organization and function of the sarcotubular machinery in ECC is thought to depend on enzymatic and/or structural activities of myotubularin which localizes to the T-tubules (6–8,13). By delivering myotubularin in the form of the fusion protein, 3E10Fv-MTM1, with anticipated affinity for muscle tissue (18,32,33), we were able to demonstrate functional and structural improvements in *Mtm1*δ4 muscle. Using only four doses of this agent over a 2-week period, we were able to confirm significant improvement in contractile-specific force in the *Mtm1*δ4 EDL muscle and observe improvements in locomotion (See Supplementary Material, Video S1). The four doses of 3E10Fv-MTM1 were also sufficient to dramatically improve the numbers of T-tubules and triads in *Mtm1*δ4 EDL myofibers, reflecting a reorganization of the sarcotubular apparatus and improved ECC as the likely mechanism behind this increase in contractile function. This represents a reversal of pre-existing sarcotubular pathology in the *Mtm1*δ4 EDL muscles, as the sarcotubular organization at 28 days of life (DOL) also shows extremely low numbers of T-tubules and triad structures (data not shown). The duration and scope of our first pilot studies were limited by the small amount of 3E10Fv-MTM1 obtained from the first round of production. As production is scaled up to produce more 3E10Fv-MTM1, studies related to dosing parameters, distribution and long-term treatment effects will be pursued. Given the positive results seen in this initial proof of concept trial of 3E10Fv-MTM1, we believe that a greater degree of functional and pathological improvement will be seen at an optimal dose and with greater duration of treatment. One potential challenge of enzyme replacement therapy is the potential for immune responses to the infused protein to limit treatment efficacy with repeated exposure to the drug. While the potential for an anti-3E10Fv-MTM1 immune response in the context of long-term treatment exists, it is encouraging to note that this has not been observed following AAV-mediated myotubularin replacement for periods of up to 1 year in mice and dogs (personal communication, Drs. Anna Buj-Bello and Martin K. Childers).

The partial positive effects of the 3E10Fv-alone control in producing higher contractile-specific force values relative to uninjected and TBS-injected animals are not readily explained; however, it is noteworthy that 3E10Fv-alone injection did not improve sarcotubular organization at the ultrastructural level, suggesting a distinct mode of action. As the ENT2 transporter has been shown to transport a number of molecules across the plasma membrane and has a high affinity for adenosine, inosine and hypoxanthine, it is possible that the use of the ENT2 transporter by 3E10Fv-alone affects the transport of these molecules to mildly improve contractile function without affecting sarcotubular organization. However, given the lack of observed muscular side effects with the long-term use of other agents that use the ENT2 transporter (such as zidovudine), it is likely that the effects of drug transport through the ENT2 transporter on muscle function are minimal. The effect of 3E10Fv-alone requires further study and will be examined further as more material becomes available and larger dosing studies ensue. Examination of

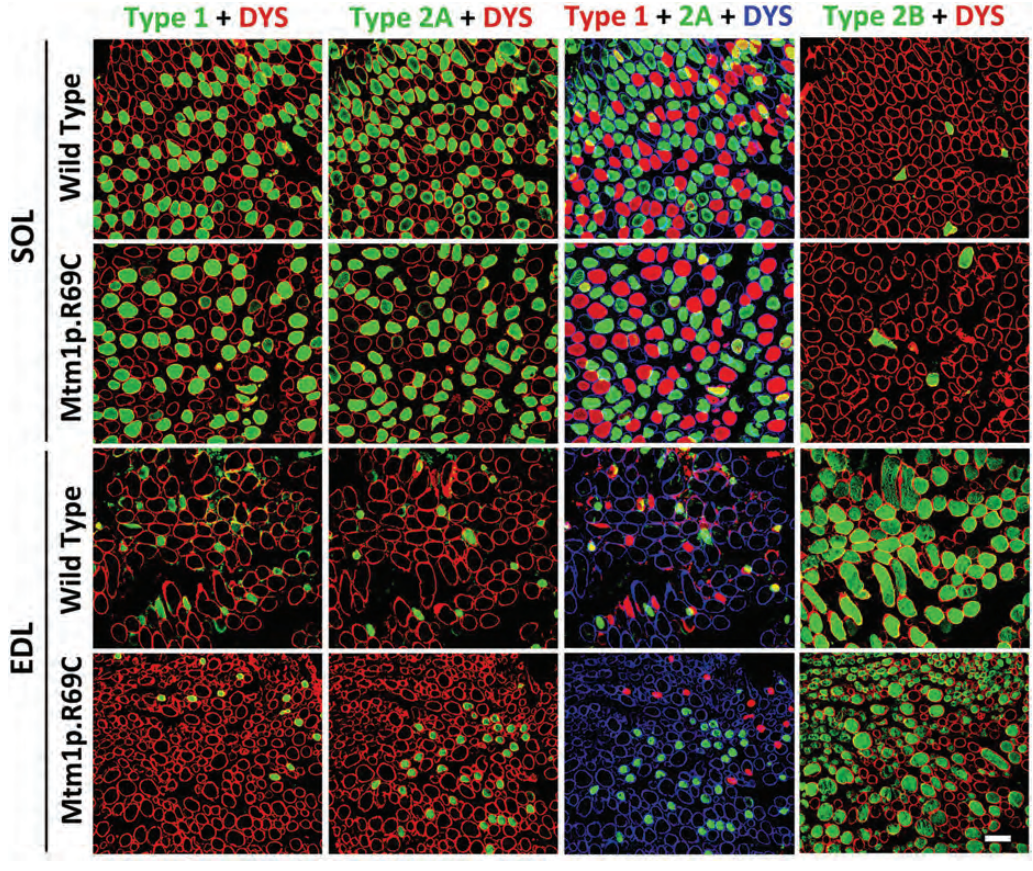

Figure 4. Immunohistochemical evaluation of fiber types in *Mtm1*p.R69C EDL and soleus muscles. Immunohistochemistry for dystrophin (red or blue) and either type 1, type 2A or 2B (green) myosin reveals the fiber-type populations present within the EDL and soleus muscles of *Mtm1*p.R69C and age-matched WT mice. Fiber-type proportions were similar in 6-week-old *Mtm1*δ4 and WT mice. A pseudocolored overlay from adjacent muscle sections stained with type 1 and 2A myosin is provided to depict the total population of oxidative fibers in these muscles. Similar distributions of oxidative and glycolytic fibers were found in WT and *Mtm1*δ4 EDL and soleus muscles at 6 weeks of life, as described in Table 2. Bar = 100 μm.

Ca^{2+} release and effects on membrane turnover and the sarcoplasmic reticulum in 3E10Fv-treated muscles should be informative in this regard.

Cell-penetrating peptides capable of delivering proteins into cells include the Antennapedia homeodomain, herpes VP22 and human immunodeficiency virus TAT (34–38). These are foreign molecules that can be toxic or induce inflammation and are not specific for muscle *in vivo* (35). Recently, additional methods for cellular entry have been described, including 'supercharging' proteins and creating 'locked' alpha-helical structures. However, these modifications are likely to disrupt activity of enzymatic proteins like myotubularin and also show no specificity for muscle uptake (35). Penetration of living cells by certain antibodies is a well-recognized phenomenon (39–42), and while some cell-penetrating antibodies produce pathological effects, the safety of mAb3E10 was demonstrated in a double-blind, placebo-controlled phase I clinical trial designed to test mab3E10 as a lupus vaccine (43). While the exact mechanism of 3E10Fv cell penetration is not yet currently understood, cellular entry specifically requires membrane expression of the human ENT2 that is particularly enriched in skeletal muscle fibers (17,18,21,32,33,43–46). Given the cell-penetrating properties of 3E10Fv, the affinity for skeletal muscle *in vivo* and the ability of various conjugates of 3E10Fv and myotubularin to maintain their respective activities, a recombinant 3E10Fv-MTM1 therapy represents a viable new approach to treat XLMTM.

MATERIALS AND METHODS

Live animal studies

All studies were performed with approval from the Institutional Animal Care and Use Committee (IACUC) at Boston Children's Hospital. *Mtm1* KO/*Mtm1*δ4 mice (5) were back-crossed for >10 generations onto a C57BL6 background. *Mtm1*p.R69C/C57BL6 mice were generated as previously described (23). Genotyping of the *Mtm1*δ4 and *Mtm1*p.R69C/C57BL6 mice was performed as previously described (5,23), and all genotypes of experimental animals refer to hemizygous males. For primary pathological and physiological evaluation, a time point of 6 weeks (42–45 DOL) was selected for *Mtm1*δ4 ($n = 6$ animals) and age-matched WT littermates ($n = 6$ animals), as this corresponds to a period of moderate-to-severe symptomatic severity in these animals. Physiological and pathological studies of *Mtm1*p.R69C mice ($n = 6$ animals) or age-matched WT littermates ($n = 6$ animals) were performed at 6 MOL, as this corresponds to a time point of stable and moderate symptomatic

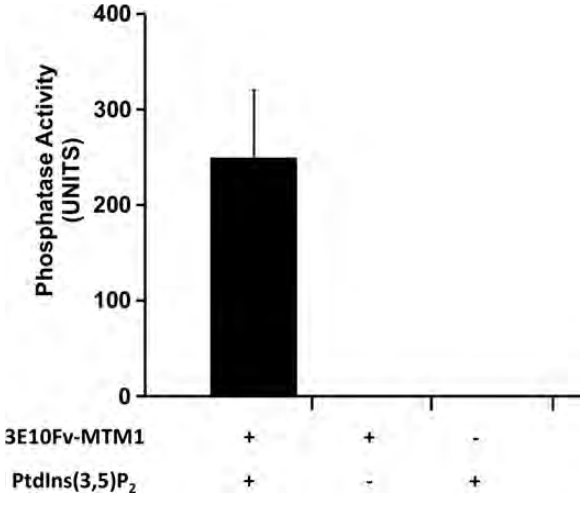

Figure 5. 3E10Fv-MTM1 possesses intact phosphatase activity. A malachite green phosphatase activity assay confirms the phosphatase activity of 100 nM 3E10Fv-MTM1expressed in, and purified from *E. coli* toward 50 μM PtdIns (3,5)P_2 over a period of 20 min at 37°C as measured in $n = 6$ reactions over two experiments. An average derived from six reactions over two experiments measured in triplicate demonstrated a mean P_i generation of 249.83 ± 70.07 pmoles per 20 μl reaction over the course of 20 min, whereas reactions deficient in enzyme and/or substrate showed no detectable P_i release. Compared with previously published data on MTM1-alone phosphatase activity (52,53), the 3E10Fv-MTM1 protein showed comparable calculated activity, especially, when considering the proportional molecular weight of myotubularin as a percentage (~70%) of the entire 3E10Fv-MTM1 fusion protein.

severity in these animals. Treatment studies were performed as described below. For all studies, animals were euthanized with carbon dioxide (CO_2) followed by cervical dislocation, per the regulations of the IACUC at Children's Hospital Boston.

Ex vivo whole muscle contractile studies

Immediately following euthanasia and external photography of the animal, the EDL and soleus muscles from WT, *Mtm1*δ4 or *Mtm1*p.R69C mice were carefully dissected and 4–0 sutures were tied around the proximal and distal tendons. The muscles were placed into heated (30°C), oxygenated (95% O_2, 5% CO_2) Krebs Henseleit buffer (pH 7.4; Sigma) containing 0.2 g of Ca^{2+} chloride and 1.8 g of sodium bicarbonate added per liter. Muscles were mounted onto a 4-channel Graz tissue bath apparatus (Harvard Apparatus) connected to a Powerlab data collection system using the Chart 5 software. Muscles were stimulated by square pulses of 0.2 ms duration at a voltage and muscle length (L0) to elicit maximal isometric twitch force. The output stimulus was derived from a Hugo Sachs Elektronik type 215E13 Voltage Pulse Generator (Harvard Apparatus) triggered at the desired frequency. Based on preliminary studies, the maximal isometric twitch response was elicited at both ages tested with a resting tension of 1.0 g and a voltage set at 10 V. Each muscle was pre-tensioned to a force of 1 g. After an initial equilibration and test stimulation period, the muscle was subjected to a tension-frequency protocol at electrical stimulation frequencies of 1, 10, 20, 30, 50, 80, 100, 120, 150 and 180 Hz, each spaced 1 min apart. The pre-tension force was reset to 1.0 g before each stimulus. After completion of the tension-frequency protocol, the length of these muscles at a pre-tension of 1.0 g was then measured, and the muscle tissue between the sutures was weighed after trimming off the suture and excess tissue. Estimated CSA was calculated by dividing the mass of the muscle (g) by the product of its length (cm) and the density of muscle (1.06 g/cm^3) (47) and expressed as square millimeters. Muscle output was expressed as specific force (mN/mm^2) determined by dividing the product of tension (g) and the acceleration of gravity (9.81 m/s^2) by muscle CSA.

Skinned single fiber studies

Mechanical properties of single skinned fiber segments were evaluated as previously described (48). Briefly, bundles of fibers from the TA, EDL and soleus muscles were chemically permeablized in a glycerol skinning solution. Single fiber segments were carefully isolated from the bundles and stored for up to 4 weeks, after which they were mounted between an isometric force transducer and high-speed motor. Fiber segments were activated by rapid transfer into an activating solution containing a free Ca^{2+} concentration of pCa 4.5 (where pCa = −log [Ca^{2+}]). Peak Ca^{2+}-activated force and unloaded shortening velocity were determined using a slack test procedure at 15°C. For analysis, force was normalized to fiber CSA (calculated from optical measurements of fiber width and depth) and shortening velocity to fiber length. Fibers were obtained from 8 *Mtm1*δ4 mice in comparison with 10 age-matched WT littermates, and from 8 *Mtm1*p.R69C mice in comparison with 9 WT littermates.

Fiber typing of single fibers

Following the physiological measurements, fiber segment myosin heavy chain isoform content was evaluated by gel electrophoresis and silver staining. Fiber segments were removed from the physiological test apparatus, placed in 10 μl of a sample buffer (containing 62.5 mM Tris (pH 6.8), 15% glycerol, 1% SDS, 15 mM dithiothreitol (DTT), 0.36 mg/ml leupeptin and 0.01% bromophenol blue) and stored at −80°C. Half of each sample was mixed with 5 μl of sample buffer and 1 μl of 1 M DTT, heated to ~95°C for 5 min and the entire volume loaded on the 4% stacking, 8% separating gel system described by Talmadge and Roy (49). Gels were run on ice in an insulated box at 80 V. After ~18 h, gels were silver stained as previously described (50).

Histological evaluation

Cross sections (8 μm) of isopentane-frozen quadriceps, EDL and soleus muscles were taken midway down the length of the muscle and stained with hematoxylin and eosin (H and E). For NADH staining, frozen sections were incubated with nitro-blue tetrazolium (1 mg/ml, Sigma) and beta-nicotinamide adenine dinucleotide (0.4 mg/ml, Sigma) in 50 mM Tris–HCl, pH 7.3, at 25°C for 30 min. Light microscopic images were captured using an Olympus DP72 camera and cellSens Standard software (Olympus, Center Valley, PA, USA). The number of centrally nucleated fibers and fibers containing subsarcolemmal mitochondrial

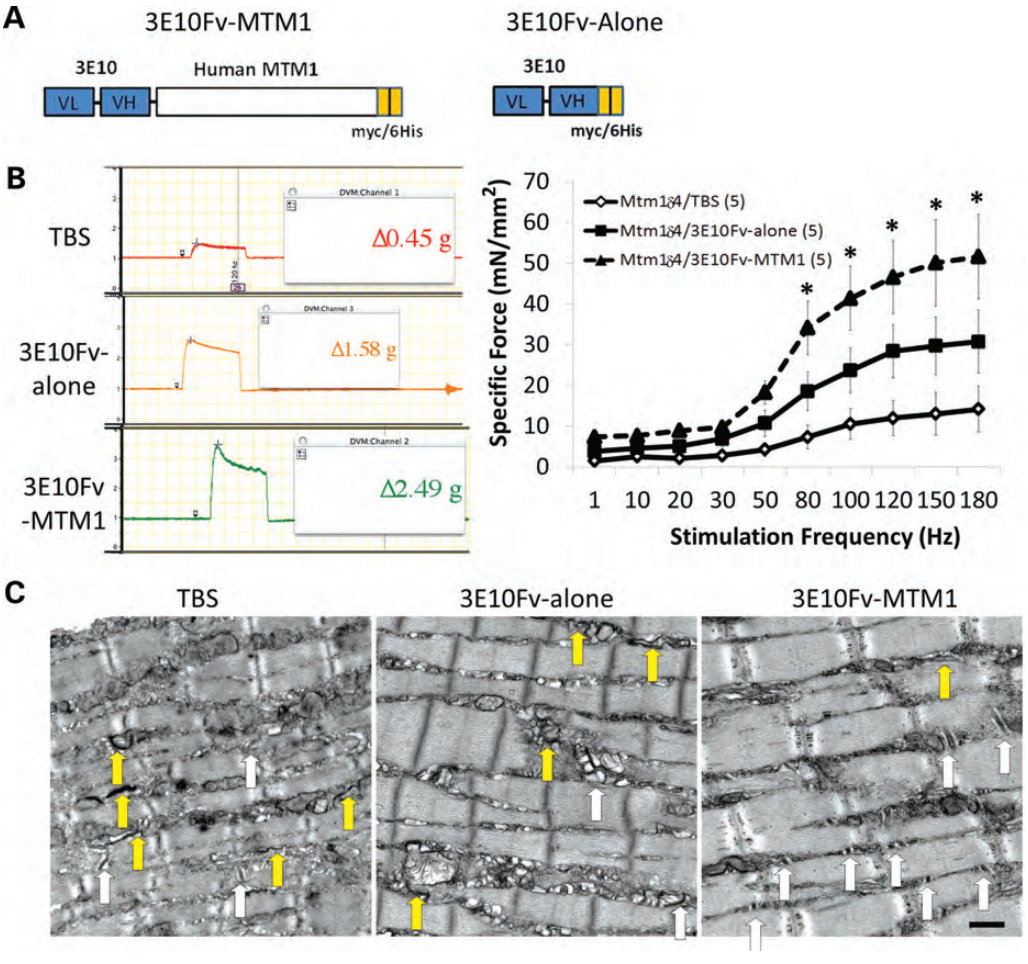

Figure 6. Improvement of functional deficits and ultrastructural abnormalities following intramuscular injection of 3E10Fv-MTM1 into *Mtm1*δ4 mice. Contractile performance was evaluated in EDL muscles of 6-week-old animals following 2 weeks of intramuscular injections into the tibialis anterior muscle with TBS, 3E10Fv-alone or 3E10Fv-MTM1. (**A**) Schematic diagrams of 3E10Fv-MTM1 and 3E10Fv-alone fusion proteins illustrating the linked V_L and V_H chains of mAB 3E10 (blue), full-length human myotubularin (white) and carboxy-terminal myc/6his tags utilized for affinity purification (orange). (**B**) Representative tracings of tetanic responses recorded at a frequency of 150 Hz depict representative maximum force in each group. Note that the vertical axes of all force tracings are on the same scale. Frequency/specific force relationships depict the force elicited in each group of animals while accounting for individual muscle cross-sectional area when expressing these data. Note that the specific force measurements for TBS-injected EDL muscles are similar to the measurements from uninjected *Mtm1*δ4 EDL muscles shown in Figure 1. $^*P < 0.01$ when comparing 3E10Fv-MTM1 to TBS injection by two-way ANOVA. (**C**) Treated animals were evaluated ultrastructurally for the presence of triads, T-tubules and L-tubules, using the same methods described in Figure 3. White arrows identify the triads and yellow arrows identify the longitudinal (L-) tubules that are identifiable in each picture. Bar = 500 nm.

aggregates were quantified by evaluating non-overlapping images of H and E or NADH stains, respectively, and manually counting the number of fibers containing these structures. For untreated mouse studies, evaluations were performed using tissue from four *Mtm1*δ4 mice in comparison with five age-matched WT littermates and from five *Mtm1*p.R69C mice in comparison with 4 WT littermates. Ultrastructural evaluations were performed on all mice that were injected with either TBS, 3E10Fv-MTM1 or 3E10Fv-alone ($n = 5$ per group).

Immunofluorescence studies

For fiber-typing studies, 8 μm frozen transverse sections of EDL or soleus muscle were double-stained with rabbit anti-dystrophin antibodies and mouse monoclonal antibodies against myosin isoforms, as previously described (14). Staining was evaluated and quantified on a Zeiss Imager Z1 (Thornwood, NY) microscope as previously described (14).

Ultrastructural studies

For electron microscopy, fixed EDL and soleus tissue was subjected to osmication, stained using uranyl acetate, dehydrated in alcohols and embedded in TAAB Epon (Marivac Ltd, Halifax, Nova Scotia, Canada). Subsequently, 1 μm scout sections of longitudinally oriented muscle were stained with toluidine blue, and evaluated for appropriate orientation. Areas of interest were cut at 95-nm thickness using an ultracut microtome (Leica Camera AG, Solms, Germany), picked up on 100-m formvar-coated copper grids, stained with 0.2% lead citrate and viewed and imaged using a Tecnai BioTwin Spirit Electron Microscope (FEI Co., Hillsboro, OR, USA). For quantitative analysis of ultrastructural features, a single well-oriented area

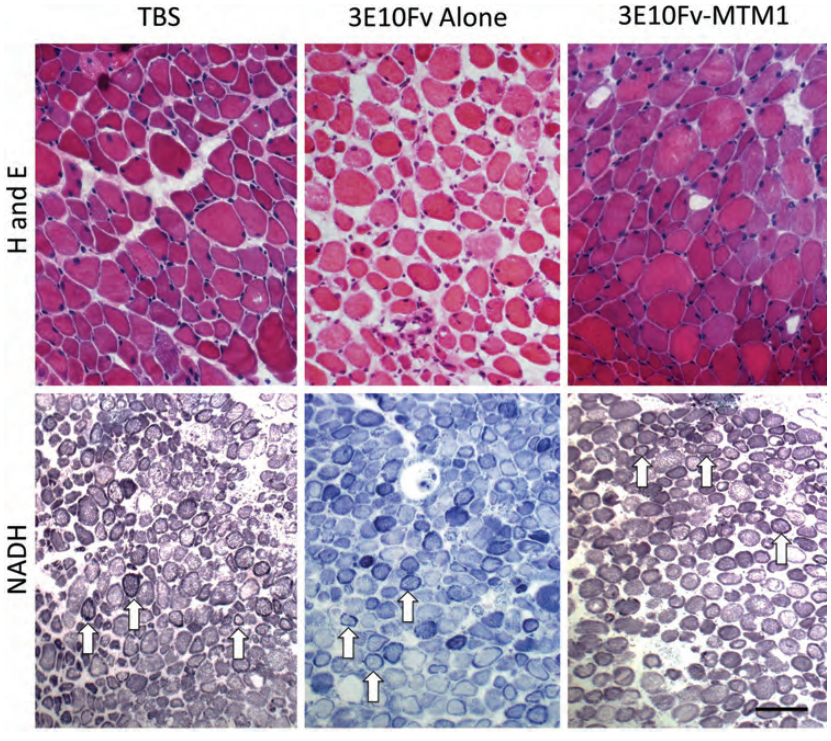

Figure 7. Pathology at the light microscopic level following 3E10Fv-MTM1 treatment of *Mtm1*δ4 mice. Hematoxylin and eosin (H and E) and NADH-TR staining of injected tibialis anterior muscles show pathological findings characteristic of myotubularin deficiency, including small fiber size, increased numbers of centrally nucleated fibers and fibers containing subsarcolemmal mitochondrial aggregates. No histological differences were noted at the light microscopic level when comparing vehicle and 3E10Fv-MTM1-injected muscles (Table 3). Arrows provide examples of fibers containing subsarcolemmal mitochondrial aggregates on NADH stain. Bar = 50μm for H and E images and 100 μm for NADH-TR images.

was selected from each fiber within the specimen (taken from two to four replicate animals for each muscle), and then photographed at ×1900, ×6800 and ×9300 magnification. The numbers of transverse (T)-tubules, triads and longitudinal (L)-tubules were quantified using the ×9300 image of each area, and these values were treated as representative of that fiber. The values from each muscle across several animals of the same genotype were then pooled for statistical analysis, and compared using ANOVA. For untreated mouse studies, evaluations were performed using tissue from two *Mtm1*δ4 mice in comparison with four age-matched WT littermates, and from four *Mtm1*p.R69C mice in comparison with two WT littermates. Ultrastructural evaluations were performed on all mice that were injected with either TBS, 3E10Fv-MTM1 or 3E10Fv-alone ($n = 5$ per group).

Production of 3E10Fv-MTM1

A gene containing an N-terminal glutathione S-transferase (GST) tag with Thrombin cleavage site and C-terminal Myc6XHis tag (GST-3E10Fv-MTM1-myc6His) was codon optimized for *E. coli* expression and *de novo* synthesized (Millipore; Temecula, CA, USA). The GST-3E10Fv-MTM1-myc6His gene was cloned into the pGEX-2T GST expression vector and transformed in an *E. coli* strain. Following expression optimization and purification with a Glutathione Sepharose 4B column, the GST tag was removed by Thrombin Cleavage. Purified 3E10Fv-MTM1-myc6His protein, named 3E10Fv-MTM1 or 4s3-001 by 4s3 Bioscience, Inc. (Concord, MA, USA), was examined for purity by SDS–PAGE, and identity was confirmed by positive reactivity with an anti-HIS mouse monoclonal antibody [#05-949;Millipore (Upstate), USA] by western blot and material was dialyzed with TBS buffer. 3E10Fv-alone was produced as a control protein in *E. coli* utilizing similar expression methods and was stored in phosphate buffered saline buffer following purification (Millipore, USA).

3E10Fv-MTM1 phosphatase assay

3E10Fv-MTM1-catalyzed dephosphorylation of phosphatidylinositol 3,5-bisphophate (PtdIns(3,5)P_2) was carried out in a 20 μl reaction mixture pH 6.5 consisting of a 1× dilution of 10× reaction buffer (0.5 M citric acid and 0.5 M NaCl) with 50 μM PtdIns(3,5)P_2 (Echelon; catalog #p-3508), 200 μM biotin-labeled phosphatidylserine (Echelon; catalog #L-31B16) and 0.05 μg of 3E10Fv-MTM1 enzyme fusion. Briefly, 3E10Fv-MTM1 enzyme or vehicle was added to reaction buffer for 2 min at 37°C before the addition of substrate and subsequent incubation time of 20 min. The reactions were terminated by the addition of 15 μl of 100 mM *N*-ethyl malemide in dimethyl sulfoxide and left at room temperature for 3 min before placing on ice and centrifuging at 8800*g* for 15 min. A portion of the supernatant (20 μl) was treated with 80 μl of Malachite green solution and assayed alongside a standard curve of inorganic phosphate (P_i) solutions according to manufacturer suggestions (Echelon, #K-1500). Color was

Table 3. Pathological evaluation of *Mtm1*δ4 tibialis anterior muscles after four doses of treatment with 3E10Fv-MTM1 or vehicle

Genotype/muscle	Fiber size (μm)	% fibers with internal nuclei	% fibers with subsarcolemmal mitochondrial aggregates	% glycolytic fibers (Type 2B)
Light microscopic studies				
TBS	24.43 ± 3.00	2.98 ± 0.62	11.12 ± 2.34	86.91 ± 3.25
3E10Fv-alone	26.84 ± 1.62	4.8 ± 0.28	10.11 ± 2.88	90.79 ± 2.51
3E10Fv-MTM1	23.62 ± 0.70	8.2 ± 2.38	10.74 ± 10.40	82.17 ± 3.80
Treatment	Fibers quantified	Triads/field	T-Tubules/field	L-Tubules/field
Ultrastructural studies				
TBS	36	4.08 ± 1.02	3.83 ± 0.99	1.38 ± 0.26
3E10Fv-alone	31	1.87 ± 0.36	1.65 ± 0.34	2.55 ± 0.29
3E10Fv-MTM1	33	10.12 ± 1.24*	8.75 ± 1.20*	2.00 ± 0.29

Injected tibialis anterior muscles were evaluated with respect to the characteristic pathological findings associated with myotubularin deficiency, using the same methods employed for Tables 2 and 3. All muscles were collected at 6 weeks of life, after receiving four doses of TBS, 3E10Fv-alone, or 3E10FV-MTM1 over a 2-week period. Data are presented as the mean ± SEM.
*$P < 0.05$.

allowed to develop for 20 min at room temperature before absorbance at 595 nm was measured, and phosphate release generated by 3E10Fv-MTM1 incubation was quantified in comparison with P_i standards.

Intramuscular injection of 3E10Fv-MTM1

Male *Mtm1*δ4 mice ($n = 5$) were injected intramuscularly into the right TA muscle with 20 μl of 0.1 mg/ml 3E10Fv-MTM1 starting at 28 DOL. This dosage was chosen based on the estimated efficacy of 3E10-delivery compared with the dose and dose interval of other non-targeted enzyme replacement therapies. Additional studies of different doses, frequencies, timing or duration of treatment were not possible due to the limited current stockpile of 3E10Fv-MTM1 material. Control male *Mtm1*δ4 mice were injected with equivalent volumes of TBS ($n = 5$) or unconjugated 3E10Fv-alone ($n = 5$) using the same dosing schedule. All animals were injected twice weekly until 42 DOL, with a total of four doses in the 2-week period. At 42 DOL, three pairs of cage-mates that had been treated with TBS and 3E10Fv-MTM1 underwent video documentation for 60 s to allow subjective comparisons of overall locomotion and disease severity. At 42 DOL, animals were euthanized, photographed, and contractile function of the right EDL muscle was evaluated using a Graz bath as described earlier. The TA, soleus, quadriceps, gastrocnemius, triceps and diaphragm muscles were carefully dissected, weighed, frozen using isopentane and stored at −80°C for subsequent histological studies. For subsequent ultrastructural studies, the entire EDL muscles and a fragment of each TA muscle were fixed in 2.5% glutaraldehyde/4% paraformaldehyde.

Statistical analysis

Statistical analyses were performed using the Prism 5 software (GraphPad Software, San Diego, CA, USA). Individual data sets were compared using ANOVA analyses and Bonferonni post tests. Differences were considered to be statistically significant at $P < 0.05$. All data are presented as means ± SEM.

SUPPLEMENTARY MATERIAL

Supplementary Material is available at *HMG* online.

Conflict of Interest statement. We would like to disclose that Dustin Armstrong is the Vice President of Research at 4s3 Bioscience, and Michael O'Callaghan is a paid consultant at 4s3 Bioscience. Both Dustin Armstrong and Michael O'Callaghan are shareholders of 4s3 Bioscience and have a financial interest in the company.

FUNDING

This work was supported by the National Institutes of Health (grant numbers P50 NS040828, R01 AR044345, K08 AR059750, K08 NS049095, L40 AR057721); the Muscular Dystrophy Association (USA) (grant numbers MDA201302, MDA155638); the Joshua Frase Foundation; the Lee and Penny Anderson Family Foundation and a Muscular Dystrophy Association Venture Philanthropy Grant Contract to 4s3 Bioscience, Inc. Antibodies for myosin type 2A and 2B were obtained from Developmental Studies Hybridoma Bank at the University of Iowa, developed under the auspices of National Institute of Child Health and Human Development. Immunofluorescence microscopy was performed using equipment at the Children's Research Institute's Imaging Core Facility at the Medical College of Wisconsin.

REFERENCES

1. Jungbluth, H., Wallgren-Pettersson, C. and Laporte, J. (2008) Centronuclear (myotubular) myopathy. *Orphanet J. Rare Dis.*, **3**, 26.
2. Heckmatt, J.Z., Sewry, C.A., Hodes, D. and Dubowitz, V. (1985) Congenital centronuclear (myotubular) myopathy. A clinical, pathological and genetic study in eight children. *Brain*, **108** (Pt 4), 941–964.
3. Pierson, C.R., Tomczak, K., Agrawal, P., Moghadaszadeh, B. and Beggs, A.H. (2005) X-linked myotubular and centronuclear myopathies. *J. Neuropathol. Exp. Neurol.*, **64**, 555–564.
4. Tsujita, K., Itoh, T., Ijuin, T., Yamamoto, A., Shisheva, A., Laporte, J. and Takenawa, T. (2004) Myotubularin regulates the function of the late endosome through the gram domain-phosphatidylinositol 3,5-bisphosphate interaction. *J. Biol. Chem.*, **279**, 13817–13824.
5. Buj-Bello, A., Laugel, V., Messaddeq, N., Zahreddine, H., Laporte, J., Pellissier, J.F. and Mandel, J.L. (2002) The lipid phosphatase

myotubularin is essential for skeletal muscle maintenance but not for myogenesis in mice. *Proc. Natl Acad. Sci. U S A*, **99**, 15060–15065.
6. Dowling, J.J., Vreede, A.P., Low, S.E., Gibbs, E.M., Kuwada, J.Y., Bonnemann, C.G. and Feldman, E.L. (2009) Loss of myotubularin function results in T-tubule disorganization in zebrafish and human myotubular myopathy. *PLoS Genet.*, **5**, e1000372.
7. Al-Qusairi, L., Weiss, N., Toussaint, A., Berbey, C., Messaddeq, N., Kretz, C., Sanoudou, D., Beggs, A.H., Allard, B., Mandel, J.L. *et al.* (2009) T-tubule disorganization and defective excitation-contraction coupling in muscle fibers lacking myotubularin lipid phosphatase. *Proc. Natl Acad. Sci. U S A*, **106**, 18763–18768.
8. Hnia, K., Tronchere, H., Tomczak, K.K., Amoasii, L., Schultz, P., Beggs, A.H., Payrastre, B., Mandel, J.L. and Laporte, J. (2011) Myotubularin controls desmin intermediate filament architecture and mitochondrial dynamics in human and mouse skeletal muscle. *J. Clin. Invest.*, **121**, 70–85.
9. Razidlo, G.L., Katafiasz, D. and Taylor, G.S. (2011) Myotubularin regulates Akt-dependent survival signaling via phosphatidylinositol 3-phosphate. *J. Biol. Chem.*, **286**, 20005–20019.
10. Lawlor, M.W., Alexander, M.S., Viola, M.G., Meng, H., Joubert, R., Gupta, V., Motohashi, N., Manfready, R.A., Hsu, C.P., Huang, P. *et al.* (2012) Myotubularin-deficient myoblasts display increased apoptosis, delayed proliferation, and poor cell engraftment. *Am. J. Pathol.*, **181**, 961–968.
11. McEntagart, M., Parsons, G., Buj-Bello, A., Biancalana, V., Fenton, I., Little, M., Krawczak, M., Thomas, N., Herman, G., Clarke, A. *et al.* (2002) Genotype-phenotype correlations in X-linked myotubular myopathy. *Neuromuscul. Disord.*, **12**, 939–946.
12. Romero, N.B. (2010) Centronuclear myopathies: a widening concept. *Neuromuscul. Disord.*, **20**, 223–228.
13. Buj-Bello, A., Fougerousse, F., Schwab, Y., Messaddeq, N., Spehner, D., Pierson, C.R., Durand, M., Kretz, C., Danos, O., Douar, A.M. *et al.* (2008) AAV-mediated intramuscular delivery of myotubularin corrects the myotubular myopathy phenotype in targeted murine muscle and suggests a function in plasma membrane homeostasis. *Hum. Mol. Genet.*, **17**, 2132–2143.
14. Lawlor, M.W., Read, B.P., Edelstein, R., Yang, N., Pierson, C.R., Stein, M.J., Wermer-Colan, A., Buj-Bello, A., Lachey, J.L., Seehra, J.S. *et al.* (2011) Inhibition of activin receptor type IIb increases strength and lifespan in myotubularin-deficient mice. *Am. J. Pathol.*, **178**, 784–793.
15. Hansen, J.E., Weisbart, R.H. and Nishimura, R.N. (2005) Antibody mediated transduction of therapeutic proteins into living cells. *ScientificWorldJournal*, **5**, 782–788.
16. Hansen, J.E., Fischer, L.K., Chan, G., Chang, S.S., Baldwin, S.W., Aragon, R.J., Carter, J.J., Lilly, M., Nishimura, R.N., Weisbart, R.H. *et al.* (2007) Antibody-mediated p53 protein therapy prevents liver metastasis in vivo. *Cancer Res.*, **67**, 1769–1774.
17. Lu, H., Chen, C. and Klaassen, C. (2004) Tissue distribution of concentrative and equilibrative nucleoside transporters in male and female rats and mice. *Drug Metab. Dispos.*, **32**, 1455–1461.
18. Pennycooke, M., Chaudary, N., Shuralyova, I., Zhang, Y. and Coe, I.R. (2001) Differential expression of human nucleoside transporters in normal and tumor tissue. *Biochem. Biophys. Res. Commun.*, **280**, 951–959.
19. Zhan, X., Ander, B.P., Liao, I.H., Hansen, J.E., Kim, C., Clements, D., Weisbart, R.H., Nishimura, R.N. and Sharp, F.R. (2010) Recombinant Fv-Hsp70 protein mediates neuroprotection after focal cerebral ischemia in rats. *Stroke*, **41**, 538–543.
20. Heinze, E., Baldwin, S., Chan, G., Hansen, J., Song, J., Clements, D., Aragon, R., Nishimura, R., Reeves, M. and Weisbart, R. (2009) Antibody-mediated FOXP3 protein therapy induces apoptosis in cancer cells in vitro and inhibits metastasis in vivo. *Int. J. Oncol.*, **35**, 167–173.
21. Weisbart, R.H., Miller, C.W., Chan, G., Wakelin, R., Ferreri, K. and Koeffler, H.P. (2003) Nuclear delivery of p53 C-terminal peptides into cancer cells using scFv fragments of a monoclonal antibody that penetrates living cells. *Cancer Lett.*, **195**, 211–219.
22. Pierson, C.R., Agrawal, P.B., Blasko, J. and Beggs, A.H. (2007) Myofiber size correlates with MTM1 mutation type and outcome in X-linked myotubular myopathy. *Neuromuscul. Disord.*, **17**, 562–568.
23. Pierson, C.R., Dulin-Smith, A.N., Durban, A.N., Marshall, M.L., Marshall, J.T., Snyder, A.D., Naiyer, N., Gladman, J.T., Chandler, D.S., Lawlor, M.W. *et al.* (2012) Modeling the human MTM1 p.R69C mutation in murine Mtm1 results in exon 4 skipping and a less severe myotubular myopathy phenotype. *Hum. Mol. Genet.*, **21**, 811–825.
24. Bevilacqua, J.A., Bitoun, M., Biancalana, V., Oldfors, A., Stoltenburg, G., Claeys, K.G., Lacene, E., Brochier, G., Manere, L., Laforet, P. *et al.* (2009) "Necklace" fibers, a new histological marker of late-onset MTM1-related centronuclear myopathy. *Acta Neuropathola*, **117**, 283–291.
25. Beggs, A.H., Bohm, J., Snead, E., Kozlowski, M., Maurer, M., Minor, K., Childers, M.K., Taylor, S.M., Hitte, C., Mickelson, J.R. *et al.* (2010) MTM1 mutation associated with X-linked myotubular myopathy in Labrador Retrievers. *Proc. Natl. Acad. Sci. U S A*, **107**, 14697–14702.
26. Laporte, J., Biancalana, V., Tanner, S.M., Kress, W., Schneider, V., Wallgren-Pettersson, C., Herger, F., Buj-Bello, A., Blondeau, F., Liechti-Gallati, S. *et al.* (2000) MTM1 mutations in X-linked myotubular myopathy. *Hum. Mutat.*, **15**, 393–409.
27. Lachmann, R.H. (2011) Enzyme replacement therapy for lysosomal storage diseases. *Curr. Opin. Pediatr.*, **23**, 588–593.
28. Julenius, K. (2007) NetCGlyc 1.0: prediction of mammalian C-mannosylation sites. *Glycobiology*, **17**, 868–876.
29. Blondeau, F., Laporte, J., Bodin, S., Superti-Furga, G., Payrastre, B. and Mandel, J.L. (2000) Myotubularin, a phosphatase deficient in myotubular myopathy, acts on phosphatidylinositol 3-kinase and phosphatidylinositol 3-phosphate pathway. *Hum. Mol. Genet.*, **9**, 2223–2229.
30. Taylor, G.S., Maehama, T. and Dixon, J.E. (2000) Myotubularin, a protein tyrosine phosphatase mutated in myotubular myopathy, dephosphorylates the lipid second messenger, phosphatidylinositol 3-phosphate. *Proc. Natl. Acad. Sci. U S A*, **97**, 8910–8915.
31. Fili, N., Calleja, V., Woscholski, R., Parker, P.J. and Larijani, B. (2006) Compartmental signal modulation: endosomal phosphatidylinositol 3-phosphate controls endosome morphology and selective cargo sorting. *Proc. Natl. Acad. Sci. U S A*, **103**, 15473–15478.
32. Hansen, J.E., Tse, C.M., Chan, G., Heinze, E.R., Nishimura, R.N. and Weisbart, R.H. (2007) Intranuclear protein transduction through a nucleoside salvage pathway. *J. Biol. Chem.*, **282**, 20790–20793.
33. Weisbart, R.H., Yang, F., Chan, G., Wakelin, R., Ferreri, K., Zack, D.J., Harrison, B., Leinwand, L.A. and Cole, G.M. (2003) Cell type specific targeted intracellular delivery into muscle of a monoclonal antibody that binds myosin IIb. *Mol. Immunol.*, **39**, 783–789.
34. Derossi, D., Joliot, A.H., Chassaing, G. and Prochiantz, A. (1994) The third helix of the Antennapedia homeodomain translocates through biological membranes. *J. Biol. Chem.*, **269**, 10444–10450.
35. McNaughton, B.R., Cronican, J.J., Thompson, D.B. and Liu, D.R. (2009) Mammalian cell penetration, siRNA transfection, and DNA transfection by supercharged proteins. *Proc. Natl Acad. Sci. U S A*, **106**, 6111–6116.
36. Prochiantz, A. (2000) Messenger proteins: homeoproteins, TAT and others. *Curr. Opin. Cell Biol.*, **12**, 400–406.
37. Schwarze, S.R., Ho, A., Vocero-Akbani, A. and Dowdy, S.F. (1999) In vivo protein transduction: delivery of a biologically active protein into the mouse. *Science*, **285**, 1569–1572.
38. Wolff, A.V., Niday, A.K., Voelker, K.A., Call, J.A., Evans, N.P., Granata, K.P. and Grange, R.W. (2006) Passive mechanical properties of maturing extensor digitorum longus are not affected by lack of dystrophin. *Muscle Nerve*, **34**, 304–312.
39. Alarcon-Segovia, D., Ruiz-Arguelles, A. and Fishbein, E. (1979) Antibody penetration into living cells. I. Intranuclear immunoglobulin in peripheral blood mononuclear cells in mixed connective tissue disease and systemic lupus erythematosus. *Clin. Exp. Immunol.*, **35**, 364–375.
40. Ma, J., Chapman, G.V., Chen, S.L., Melick, G., Penny, R. and Breit, S.N. (1991) Antibody penetration of viable human cells. I. Increased penetration of human lymphocytes by anti-RNP IgG. *Clin. Exp. Immunol.*, **84**, 83–91.
41. Tan, E.M. and Kunkel, H.G. (2006) Characteristics of a soluble nuclear antigen precipitating with sera of patients with systemic lupus erythematosus. J. Immunol. 1966. 96: 464–471. *J. Immunol*, **176**, 1297–1304.
42. Yanase, K., Smith, R.M., Cizman, B., Foster, M.H., Peachey, L.D., Jarett, L. and Madaio, M.P. (1994) A subgroup of murine monoclonal anti-deoxyribonucleic acid antibodies traverse the cytoplasm and enter the nucleus in a time-and temperature- dependent manner. *Lab. Invest.*, **71**, 52–60.
43. Spertini, F., Leimgruber, A., Morel, B., Khazaeli, M.B., Yamamoto, K., Dayer, J.M., Weisbart, R.H. and Lee, M.L. (1999) Idiotypic vaccination with a murine anti-dsDNA antibody: phase I study in patients with nonactive systemic lupus erythematosus with nephritis. *J. Rheumatol.*, **26**, 2602–2608.

44. Crawford, C.R., Patel, D.H., Naeve, C. and Belt, J.A. (1998) Cloning of the human equilibrative, nitrobenzylmercaptopurine riboside (NBMPR)-insensitive nucleoside transporter ei by functional expression in a transport-deficient cell line. *J. Biol. Chem.*, **273**, 5288–5293.
45. Weisbart, R.H., Stempniak, M., Harris, S., Zack, D.J. and Ferreri, K. (1998) An autoantibody is modified for use as a delivery system to target the cell nucleus: therapeutic implications. *J. Autoimmun.*, **11**, 539–546.
46. Zack, D.J., Stempniak, M., Wong, A.L., Taylor, C. and Weisbart, R.H. (1996) Mechanisms of cellular penetration and nuclear localization of an anti-double strand DNA autoantibody. *J. Immunol.*, **157**, 2082–2088.
47. Mendez, J. and Keys, A. (1960) Density and composition of mammalian muscle. *Metabolism*, **9**, 184–188.
48. Choi, S.J. and Widrick, J.J. (2010) Calcium-activated force of human muscle fibers following a standardized eccentric contraction. *Am. J. Physiol. Cell Physiol.*, **299**, C1409–1417.
49. Talmadge, R.J. and Roy, R.R. (1993) Electrophoretic separation of rat skeletal muscle myosin heavy-chain isoforms. *J. Appl. Physiol.*, **75**, 2337–2340.
50. Giulian, G.G., Moss, R.L. and Greaser, M. (1983) Improved methodology for analysis and quantitation of proteins on one-dimensional silver-stained slab gels. *Anal. Biochem.*, **129**, 277–287.
51. Grange, R.W., Gainer, T.G., Marschner, K.M., Talmadge, R.J. and Stull, J.T. (2002) Fast-twitch skeletal muscles of dystrophic mouse pups are resistant to injury from acute mechanical stress. *Am. J. Physiol. Cell. Physiol.*, **283**, C1090–1101.
52. Schaletzky, J., Dove, S.K., Short, B., Lorenzo, O., Clague, M.J. and Barr, F.A. (2003) Phosphatidylinositol-5-phosphate activation and conserved substrate specificity of the myotubularin phosphatidylinositol 3-phosphatases. *Curr. Biol.*, **13**, 504–509.
53. Tronchere, H., Laporte, J., Pendaries, C., Chaussade, C., Liaubet, L., Pirola, L., Mandel, J.L. and Payrastre, B. (2004) Production of phosphatidylinositol 5-phosphate by the phosphoinositide 3-phosphatase myotubularin in mammalian cells. *J. Biol. Chem.*, **279**, 7304–7312.
54. Goodman, C.A., Blazev, R., Kemp, J. and Stephenson, G.M. (2008) E-C coupling and contractile characteristics of mechanically skinned single fibres from young rats during rapid growth and maturation. *Pflugers Archiv*, **456**, 1217–1228.